Mathematical Biosciences and Engineering

https://www.aimspress.com/journal/mbe

MBE, 23(1): 97–123.
DOI: 10.3934/mbe.2026005
Received: 29 July 2025
Revised: 29 October 2025
Accepted: 21 November 2025
Published: 28 November 2025

Research article

Base state of growing reaction-dilution systems exhibiting Turing patterns

Aldo Ledesma-Durán *, Consuelo García-Alcántara and Iván Santamaría-Holek

Unidad Multidisciplinaria de Docencia e Investigación, Universidad Nacional Autónoma de México, Boulevard Juriquilla 3001, Juriquilla, 76230, Querétaro, Mexico

* **Correspondence:** Email: aldo_ledesma@ciencias.unam.mx; Tel: +52-442-192-6207.

Abstract: Turing pattern formation in growing domains depends on a steady state that balances reaction rates and local volume changes, leading to more complex patterning conditions than in fixed domains. We analyzed the effects of domain growth and shrinkage on spatially homogeneous concentrations and their stability, demonstrating that long-term behavior depends on the growth type: exponential growth causes asymptotic deviations, linear and quadratic growth enable gradual recovery of the fixed-domain state, and oscillatory growth induces concentration oscillations. Using a linear approximation for the base state, we derived an analytic expression that accurately predicts these effects for slow domain variations. Our theoretical model shows that dilution-induced steady states evolve proportionally to the chemical fixed-point concentration, a result validated through extensive numerical simulations of the Brusselator and BVAM reactions. Additionally, we proposed an approximate framework for evaluating the stability of spatially homogeneous perturbations, interpreting it as a balance between reaction rates and dilution. This yielded an analytical criterion for determining stability in the absence of diffusion, offering an alternative to previously exclusive numerical approaches for identifying the first Turing condition for pattern formation.

Keywords: Turing pattern; growing domain; Lyapunov function; base state; homogeneous

1. Introduction

The Turing mechanism for pattern formation posits that the interaction between two chemical substances—typically an activator and an inhibitor—can give rise to complex, repetitive spatial structures such as spots or stripes, which are characteristic of a wide range of biological systems [1]. These patterns are not only responsible for external morphological traits, such as animal coloration, but also play a critical role in fundamental developmental processes, including the formation of organs and tissues [2]. Turing instability arises from a reaction-diffusion process, whose dynamics allow for the prediction of structured patterns emerging from initially homogeneous conditions. However, unlike the

classical Turing model, which assumes fixed spatial domains, biological patterns often arise in growing media [3, 4]. This growth introduces dilution effects and changes in the spatial distribution of interacting substances, which significantly influence the shape and arrangement of the resulting patterns.

Understanding pattern formation in expanding domains is not only of theoretical interest but also holds considerable practical relevance: in regenerative medicine, it enables the exploration of strategies to control and guide the development of functional tissue structures [5, 6]; in materials science, it inspires the design of self-organized materials with tailored properties [7]; and in evolutionary biology, it provides a framework for understanding how developmental processes contribute to morphological diversification in response to environmental pressures [8, 9].

The effects of changing domain size on reaction concentrations have significant real-world implications, particularly in biological systems where a system's volume, such as a growing cell or tissue, changes dynamically. Our analysis reveals that linear or quadratic domain expansions are compatible with stable biological processes such as cell growth and division. This is because they provide a mechanism for cells to counteract the dilution effects that result from an increase in volume, allowing their internal environment to remain stable and healthy [10, 11]. In contrast, the understanding of uncontrolled expansion in tumors, where the rapid increase in volume prevents the system from reaching a stable state and leads to the dysregulation of key chemical processes, could be modeled with exponential growth domains that lead to unstable asymptotic deviations [12, 13]. Additionally, the framework presented in this work has practical relevance for explaining the activity of GTPases in processes like growth factor-stimulated fibroblasts and neuronal cells [14], as well as their temporal activation during neurite outgrowth [15] and cell protrusion [16]. Thus, models based on the Turing mechanism offer a powerful tool for addressing fundamental questions regarding self-organization, adaptation, and evolution in both natural and synthetic systems.

In recent years, significant progress has been made in understanding how domain growth, domain shape (or manifold evolution), and additional mechanisms such as chemotaxis or concentration-dependent evolution affect Turing pattern formation. Waters et al. [17] considered hybrid apical–uniform domain growth and demonstrated how growth distributions influence pattern wavelength and orientation under continuously expanding domains. Earlier work in [18] similarly analyzed reaction-diffusion systems on non-autonomous growing domains, showing that time-dependent domain size can alter stability thresholds. More recent studies include [19], which introduced spatially inhomogeneous feed rates in a Schnakenberg-type system and showed that heterogeneity induces novel spot creation–destruction loops and strongly modulates spot density and height. Moreover, Krause et al. [20] studied concentration-dependent domain evolution in one and higher dimensions, finding that when growth depends on morphogen concentration, rapid growth or contraction leads to new phenomena near bifurcation boundaries, often beyond what linear stability predicts. Another line of work in [21] incorporated chemotaxis coupled with reaction-diffusion, finding that chemotactic coupling can expand the parameter region for pattern formation and accelerate pattern emergence, though sometimes at the cost of reduced spatial regularity. Together, these results underscore that domain growth type (uniform vs. apical vs. concentration-driven), spatial heterogeneity, and added dynamics such as chemotaxis qualitatively and quantitatively shift both the onset of Turing-type instabilities and the resulting pattern geometries. Moreover, Silva-Dias et al. [22] reported the formation of single and multiple stationary spiral patterns, along with transitional patterns, in the CDIMA (chlorine dioxide–iodine–malonic acid) reaction. They analyzed the relationship between the final morpholo-

gies and the radial and angular growth velocities, examined the importance of the size of the initial nucleation site in determining spiral multiplicity, and evaluated the stability and robustness of these Turing patterns.

Evidence from numerical simulations shows that the shape of the pattern in a growing domain at a specific time depends on its history [23, 24]. It was conjectured that this type of memory is determined by the ability of a dissipative structure to maintain a wavenumber, even when there is another wavenumber that may be more stable to sideband perturbances [25–27]. To test this hypothesis, a non-linear approximation to the solution of the reaction-diffusion-dilution (RDD) system near the Turing bifurcation is required. However, despite important progress made in establishing the conditions for the emergence of Turing patterns in growing domains [18, 28–30], this remains an open problem.

The first difficulty in finding the conditions for the emergence of Turing patterns in increasing domains is that the spatial homogeneous state, that is, the state of the system in the absence of diffusion, itself depends on time [30]. The homogeneous state is the basis for analyzing pattern formation in reaction–diffusion systems. In classical Turing theory, it must remain stable to uniform perturbations but become unstable to spatial ones at critical parameter values, ensuring that patterns arise purely from diffusion effects. Yet, factors like domain size and boundary conditions can trigger instabilities even when this condition is not met, revealing alternative self-organization mechanisms [31, 32]. This contrast underscores the key role of homogeneous state stability in understanding pattern formation. Approximations to the homogeneous reference state are almost non-existent in the literature. An exception is the work in [33], where the time dependence of the homogeneous state is assumed to change little and can therefore be assumed to be replaceable by an average value. However, the time dependency has several consequences. The first is that all spatial perturbations present in the system are referred to this state and, therefore, they could store information about the inertia of the system in their development, complicating the problem of determining its stability. The second issue has to do with the stability of the homogeneous state itself since, as we will see in this work, it may not tend asymptotically to any value, it may show initial temporal variations independently of the initial condition, and it may even give rise to unstable states even when the chemical reaction would be stable in a fixed domain. This is in contrast to what happens with a fixed-length domain where the reaction fixed point defines the steady homogeneous state with which simulations are initialized and around which spatial perturbations occur.

With this in mind, a study of the conditions in Turing patterns in growing domains must first consider this base state that directly affects the stability of the spatial perturbations that define the bifurcation, and until now has only been studied numerically, see, for example, [30]. This work is the first systematic and formal study we know of in this regard, and is essential to obtain closed analytical conditions for Turing instability. To simplify some methodological aspects, we will focus on a one-dimensional RDD system in a Euclidean space under the hypothesis of isotropic growth, i.e., a growth that occurs in the same way in each region of the domain. Aspects that complicate the presentation but do not modify the basic aspects of this deduction, such as the use of more spatial dimensions or the use of different boundary conditions, are not considered in this work.

This work aims to understand general aspects of the base state under different growth dynamics such as exponential, linear, quadratic, and sinusoidal. To do so, we will derive an approximate expression for the solution when the growth rate is relatively slow compared to the characteristic reaction and diffusion times of the system, which is the case in most biological applications such as the appearance

of patterns on animal skin. We will validate this expression by finite element simulations on the reaction systems of the Brusselator [34] and BVAM [35] models. In addition, we will also consider the domain shrinkage option, which has been scarcely considered so far.

The main outcome of our discussion will focus on understanding the stability of perturbations to the base state, which constitutes the first Turing condition for the emergence of spatial patterns. We find that, unlike what happens in a fixed-size domain, in a growing domain, the response to a spatially homogeneous disturbance combines the competition between the local production/consumption rates of the reaction and the local change of volume introduced by dilution. The local production/consumption rates describe the net contribution of the reaction terms, i.e., the rate at which each component is locally generated or depleted as a result of the underlying chemical kinetics. In contrast, the volume changes not only affect the steady state but could also change the dynamical properties of the perturbations giving rise to new possible stability changes that could lead to the appearance/disappearance of Turing patterns that do not occur in a fixed domain. In this work we focus only on the base state, which has been studied only numerically in other works on Turing patterns in growth domains, see, for example, [30, 36, 37].

The structure of this work is as follows. In Section 2, we present the RDD systems and distinguish the equations for the base state and the perturbations. In Section 3, we provide a formal solution for the spatially homogeneous state based on a linear approximation. We also discuss when this time-dependent solution can be approximated by a constant solution for the exponential, linear quadratic, and oscillatory cases. In Section 4, we test our prediction for the Brusselator and provide numerical evidence for the validity of our approximation. Based on these considerations, in Section 5, we discuss how the combined effect of reaction rates and dilution explain the stability properties of homogeneous perturbations. Finally, in Section 6, we present a summary of conclusions and discuss the perspective of our results.

2. Base state and perturbations of the RDD system in a dynamic domain

Consider a set of chemical species summarized in the vector $\mathbf{c}(x,t)$, all diffusing in a one-dimensional domain that grows homogeneously with time t and has size $l(t)$ on a Euclidean line. The x coordinate determines a position in the physical domain. The RDD equation describing the process is [38]

$$\frac{\partial \mathbf{c}}{\partial t} + \frac{\dot{l}(t)}{l(t)}\mathbf{c}(x,t) = \mathbb{D}\frac{\partial^2 \mathbf{c}}{\partial x^2} + \mathbf{f}(\mathbf{c}). \tag{2.1}$$

In this equation, $\mathbb{D}$ is the diffusion coefficient matrix which, without loss of generality, can be taken as diagonal. Here, we introduced the local production/consumption of particles per unit length and time as $\mathbf{f}(\mathbf{c}(x,t))$, measuring the local rate of the reaction for each component and therefore independent of the domain size. We focus for this study on zero-flow boundary conditions and on initial conditions with perturbations close to the fixed-point concentration as detailed below.

If the local volume change is homogeneous throughout the domain (isotropic growth), the relationship between the moving and fixed reference system with coordinates ξ is $x = l(t)\xi$ with $\xi \in [0,1]$.

Using this transformation [37], the last equation becomes

$$\frac{\partial \mathbf{c}}{\partial t} + g(t)\mathbf{c}(\xi, t) = \frac{1}{l^2(t)}\mathbb{D}\frac{\partial^2 \mathbf{c}}{\partial \xi^2} + \mathbf{f}(\mathbf{c}). \tag{2.2}$$

Here we define $g(t) \equiv \dot{l}(t)/l(t)$ to represent the growth rate per unit length, as it can be approximated as $g(t) \approx \Delta l/(l\Delta t)$. This equation is applicable to the one-dimensional RDD process on a Euclidean domain growing isotropically [38]. More general frameworks and deductions including curved domains or anisotropic growth can be found in [37–39].

Regarding chemical reactions, in our work we will use the Brusselator and BVAM reaction models to exemplify our results [34, 40, 41]. Therefore, if $\mathbf{c} = (c_u, c_v)^T$, the reaction are:

$$\mathbf{f}_B(\mathbf{c}) = (A - Bc_u - c_u + c_u^2 c_v, Bc_u - c_u^2 c_v)^T, \tag{2.3}$$

$$\mathbf{f}_{BVAM}(\mathbf{c}) = (c_u + ac_v - c_u c_v - c_u c_v^2, bc_v + hc_u + c_u c_v + c_u c_v^2)^T. \tag{2.4}$$

These equations are derived from the law of mass action and, as we will show, lead to very different base states due to their different interpretation.

The homogeneous state around which perturbations are studied is different in a domain that grows relative to one of fixed size. When studying Turing bifurcation on fixed domains, one considers the stability of spatial perturbations around a fixed-point concentration $\mathbf{c}_0$, defined by setting all reaction rates equal to zero, $\mathbf{f}(\mathbf{c}_0) = \mathbf{0}$. In open systems (such as the Brusselator), this fixed point is usually not the origin, but a steady state defined by $\mathbf{c}_0$ to which concentrations will asymptotically tend.

On the contrary, for a dynamic domain, if we consider a perturbation $\boldsymbol{\zeta}(\xi, t) = \mathbf{c}(\xi, t) - \mathbf{c}_s(t)$ around a homogeneous quasi-equilibrium state $\mathbf{c}_s(t)$, then it follows from the equation (2.2) that

$$\frac{\partial \mathbf{c}_s}{\partial t} + g(t)\mathbf{c}_s - \mathbf{f}(\mathbf{c}_s) = -\frac{\partial \boldsymbol{\zeta}}{\partial t} - g(t)\boldsymbol{\zeta} + \frac{1}{l^2(t)}\mathbb{D}\frac{\partial^2 \boldsymbol{\zeta}}{\partial \xi^2} + \frac{\partial \mathbf{f}}{\partial \mathbf{c}}(\mathbf{c}_s)\boldsymbol{\zeta} + O(\boldsymbol{\zeta}^2), \tag{2.5}$$

where we have expanded the function $\mathbf{f}(\mathbf{c})$ in series around $\mathbf{c}_s$. Neglecting quadratic terms in the perturbations, the previous equation leads to two problems. The first one allows us to determine the quasi-equilibrium homogeneous state $\mathbf{c}_s(t)$ from

$$\frac{\partial \mathbf{c}_s}{\partial t} + \frac{\dot{l}(t)}{l(t)}\mathbf{c}_s = \mathbf{f}(\mathbf{c}_s). \tag{2.6}$$

The second problem allows us to determine the disturbance dynamics:

$$\frac{\partial \boldsymbol{\zeta}}{\partial t} + \frac{\dot{l}(t)}{l(t)}\boldsymbol{\zeta} = \frac{1}{l^2(t)}\mathbb{D}\frac{\partial^2 \boldsymbol{\zeta}}{\partial \xi^2} + \frac{\partial \mathbf{f}}{\partial \mathbf{c}}(\mathbf{c}_s)\boldsymbol{\zeta}. \tag{2.7}$$

The solution of this equation requires the prior determination of $\mathbf{c}_s$ for the evaluation of the Jacobian term $\frac{\partial \mathbf{f}}{\partial \mathbf{c}}(\mathbf{c}_s)$. Therefore, the determination of the Turing patterns via equation (2.7) for perturbations crucially depends on the evaluation of the quasi-equilibrium state in (2.6).

Equation (2.6) is a nonlinear problem that cannot be solved analytically in general, and for which some trends have been illustrated based on numerical solutions for some types of growth and reaction systems, see, for example, [30]. In the next section, we obtain a formal approximation for the base state solution in (2.6) to understand in a completely general way its properties as soon as some linearity assumptions are fulfilled.

3. Linear approximation to the quasi-equilibrium base state

To approximate solutions to the nonlinear problem (2.6), we assume that, if the growth is not too fast, the average concentration also varies slowly compared to that of a fixed-sized domain. Thus, the stability of the system can be analyzed by small perturbations around this state. Although this assumption is not always valid, our numerical results show that, in most cases with slow growth, it is a good approximation. Therefore, the behavior of the base state can be described with a linear approach.

3.1. Time-dependent homogeneous state

Let us find an approximate solution of (2.6) assuming that the concentration values are already close to the fixed-point concentration $\mathbf{c}_0$ where $\mathbf{f}(\mathbf{c}_0) = \mathbf{0}$. In this case, the reaction can be approximated as $\mathbf{f}(\mathbf{c}_s) \approx \mathbb{J}[\mathbf{c}_s(t) - \mathbf{c}_0]$ where $\mathbb{J}$ is the constant Jacobian matrix of the reaction evaluated at $\mathbf{c}_0$. Defining the deviations around the homogeneous state as $\delta\mathbf{c}(t) = \mathbf{c}_s(t) - \mathbf{c}_0$, this leads to

$$\frac{d\,[\delta\mathbf{c}]}{dt} + g(t)[\mathbf{c}_0 + \delta\mathbf{c}] \approx \mathbb{J}\,\delta\mathbf{c}. \tag{3.1}$$

If $\mathbb{J}$ is a diagonalizable constant square matrix with modal matrix $\mathbb{P}$ such that $\mathbf{\Lambda} = \mathbb{P}^{-1}\mathbb{J}\mathbb{P}$, then the solution of this linear non-homogeneous differential equation in (3.1) with initial condition $\delta\mathbf{c}(0)$ is

$$\delta\mathbf{c} = \frac{l(0)}{l(t)}\mathbb{P}e^{\mathbf{\Lambda}t}\mathbb{P}^{-1}\delta\mathbf{c}(0) - \mathbb{P}\frac{e^{\mathbf{\Lambda}t}}{l(t)}\left(\int_0^t l'(t')e^{-\mathbf{\Lambda}t'}dt'\right)\mathbb{P}^{-1}\mathbf{c}_0, \tag{3.2}$$

with $\mathbf{\Lambda}$ the diagonal matrix whose entries are the eigenvalues of $\mathbb{J}$. The derivation of this solution is given in Appendix A of the Supplementary material.

Equation (3.2) states that the deviation of the homogeneous state $\mathbf{c}_s$ from the fixed-point concentration $\mathbf{c}_0$ has two terms:

- A contribution proportional to the initial deviation $\delta\mathbf{c}(0)$ that will decay exponentially due to terms of the form $e^{\Lambda_i t}/l(t)$, where Λ_i is the i-th element of the diagonal of $\mathbf{\Lambda}$. This contribution represents the competition between the tendency of the reaction to the production/consumption of material, (measured by the terms $e^{\Lambda_i t}$) and the dilution effect (measured by $l(t)$) which may increase or decrease the volume depending on the type of growth.
- A proportional contribution to the fixed-point concentration $\mathbf{c}_0$. The magnitude of this deviation is, in turn, proportional to the factor $e^{\Lambda_i t}\left(\int_0^t l'(t')e^{-\Lambda_i t'}dt'\right)/l(t)$ and, as we will show, is most pronounced at the beginning of the process for growing domains and toward the end for shrinking domains.

The first contribution for the homogeneous state depends on the initial conditions and can be set to zero without loss of generality. The second indicates that in a reactor with a continuous inflow of material, the concentration does not immediately reach a steady state but fluctuates over time based on the given factor. This equilibrium depends on the type and rate of growth.

Taking this into account, from the result in (3.2), assuming that the system is already initially at the fixed-point concentration $\mathbf{c}_0$, then $\delta\mathbf{c}(0) = 0$, and the homogeneous state obeys

$$\mathbf{c}_s \approx \left[\mathbb{I} - \mathbb{P}\frac{e^{\mathbf{\Lambda} t}}{l(t)}\left(\int_0^t \dot{l}(t')e^{-\mathbf{\Lambda} t'}dt'\right)\mathbb{P}^{-1}\right]\mathbf{c}_0. \tag{3.3}$$

This equation is approximate since it consists of a linearization of $\mathbf{f}(\mathbf{c}_s)$ around $\mathbf{c}_0$ as (3.1) is the linear approximation of (2.6). Later in our numerical examples, we will see what factors could contribute to the problem's nonlinearity and, therefore, to the possible failure of (3.3).

3.2. Expected error and scope of the approximation

In order to estimate the error of the approximate formula in (3.3), we substitute this expression plus an error term $\mathbf{e}(t)$ into equation (2.6). After some algebraic manipulation this leads to

$$\mathbf{e}'(t) = (\mathbf{\Lambda} - g(t)\mathbf{I})\,\mathbf{e}(t) + \Big[\mathbf{f}(\mathbf{c}_s) - \mathbf{\Lambda}(\mathbf{c}_s - \mathbf{c}_0)\Big], \tag{3.4}$$

which constitutes a non-autonomous system of equations describing the error.

The first term defines a set of decoupled equations for each error component. The solution of the homogeneous part is

$$\mathbf{e}_i(t) = \exp\left[\Lambda_i t - \log\frac{l(t)}{l(0)}\right]\mathbf{e}_i^0. \tag{3.5}$$

The homogeneous part of the equation establishes that the error of the approximation in (3.3) tends to zero provided that $\mathcal{R}e[\Lambda_i]t - \log\left(\frac{l(t)}{l(0)}\right) < 0$. This condition, which will be derived and explained in detail below, implies that the approximation error tends to zero provided that the dilution measured by $l(t)$ is limited in a specific way by the intrinsic growth rate of the chemical reactions in the absence of growth, represented by the real part of the eigenvalues $\mathcal{R}e[\Lambda_i]$.

The second term in (3.4) is independent of the error and has the generic form $\mathbf{f}(\mathbf{c}) - \mathbf{\Lambda}(\mathbf{c} - \mathbf{c}_0)$, so it only involves the net reaction rates. This means that the solution obtained using the full reaction rate, including the nonlinear terms and denoted by $\mathbf{f}(\mathbf{c})$, can be represented by a homeomorphism, where the dynamics are mainly determined by the linearization. Consequently, the convergence of the error to zero is guaranteed in principle, provided that the assumptions of the Hartman–Grobman theorem hold, namely that $\mathbf{c}_0$ is a hyperbolic equilibrium point and $\mathbf{f}$ is a smooth map. For the purposes of this work, it is sufficient to require that $\int_0^t [\mathbf{f}(\mathbf{c}) - \mathbf{\Lambda}(\mathbf{c} - \mathbf{c}_0)]\,dt < \boldsymbol{\epsilon}_0 e^{-jt}$, for some $j > 0$ and for all t. Under the conditions of these two paragraphs, the asymptotic convergence of the error in (3.4) to zero is guaranteed.

Equation (3.4) also allows us to anticipate scenarios where the approximation in (3.3) may fail. This occurs when the shrinkage is very fast, i.e., when $l(t) < l(0)e^{\mathcal{R}e[\Lambda_i]t}$ for all i, in which case dilution is much slower than the damping of the perturbations and the material accumulates; when the reaction parameters place the fixed-point solution close to a bifurcation where $\mathcal{R}e[\Lambda_i]$ vanishes while the domain is growing; and finally, when the nonlinear terms cannot be approximated by the linear part, which could happen for very rapid growth capable of altering the hyperbolic nature of the original fixed point (that would exist in the absence of growth). All of these scenarios are confirmed by our numerical simulations. However, for most of the cases used in Turing simulations of biological systems where the growth rate is very slow, the approximation seems sufficiently accurate. In cases of rapid growth, the approximation would have to be modified or the general equation (2.6) used in any case to account for the accelerated growth-decline dynamics.

3.3. Explicit computation for some types of growing

To make analytic progress, the expression (3.3) can be computed explicitly for some functions $l(t)$ along these general lines: Given $l(t)$ as an exponential, sinusoidal, or polynomial function, integrals of the form $e^{\Lambda_i}/l(t)\int_0^t e^{\Lambda_i t} l'(t')dt'$ can be computed explicitly, yielding rational functions similar to $l(t)$ in numerator and denominator, and in terms of powers of the eigenvalues Λ_i^m. Since all matrices involving $\mathbf{\Lambda}$ in (3.3) are diagonal, the scalar result can be converted to a diagonal matrix using direct replacement of $\Lambda_i \to \mathbf{\Lambda}$. Then, using the properties of the modal matrix, all terms in the matrix $\mathbb{P}\mathbf{\Lambda}^m\mathbb{P}^{-1}$ are replaced by terms of the form $\mathbb{J}^m$. This allows us to find the explicit expression for $\mathbf{c}_s$ for these types of growth. This procedure is exemplified for quadratic growth in Appendix B of the Supplementary material.

Table 1. The temporal deviation of the homogeneous state from the fixed point $\mathbf{c}_0$ in (3.6) for different types of growth in the first column.

Size ratio $l(t)/l(0)$	Deviation $\boldsymbol{\delta C}(t)$
e^{rt}	$r(\mathbb{J}-r\mathbb{I})^{-1}(\mathbb{I}-e^{\mathbb{J}t}e^{-rt})$
$1+rt$	$\frac{r}{1+rt}\mathbb{J}^{-1}\left(\mathbb{I}-e^{\mathbb{J}t}\right)$
$1+rt^2$	$\frac{2r}{1+rt^2}\mathbb{J}^{-2}\left(\mathbb{I}-e^{\mathbb{J}t}+t\mathbb{J}\right)$
$1+r\sin(\omega t)$	$\frac{r\omega}{1+r\sin(\omega t)}(\mathbb{J}^2+\omega^2\mathbb{I})^{-1}[\mathbb{J}\cos(\omega t)-\omega\sin(\omega t)-\mathbb{J}e^{\mathbb{J}t}]$

We have performed this computation for exponential, linear, quadratic, and sinusoidal growth. From (3.3), we can write

$$\mathbf{c}_s - \mathbf{c}_0 = \boldsymbol{\delta C}(t)\,\mathbf{c}_0, \tag{3.6}$$

and the form of this matrix $\boldsymbol{\delta C}(t)$ that measures the deviation between the base state and the fixed-point concentration is given in Table 1. Some properties are:

- *General traits.* The deviation between the base state and the fixed point is proportional to r, the parameter measuring how fast the domain grows. The damping of the solution depends on the eigenvalues of the Jacobian matrix evaluated at $\mathbf{c}_0$ through the exponential factor $e^{\mathbb{J}t}$, so the stability of the homogeneous state partially inherits the local stability of the chemical reaction. Furthermore, the deviation is proportional to some term depending on negative powers of $\mathbb{J}$ (or some modification), meaning that if any of the eigenvalues of $\mathbb{J}$ are close to zero and hence close to a bifurcation, the deviations from $\boldsymbol{\delta C}(t)$ could be large.
- *Particular traits.* For the exponential case, the deviation from the fixed-point concentration for long times is proportional to constant values, so the steady state can be different from the fixed point. For linear growth, if the eigenvalues of $\mathbb{J}$ have a negative real part, the deviation decays to zero as $r/(1+rt)$, and something similar occurs for quadratic growth with rate $rt/(1+rt^2)$; therefore in these two cases, in an increasing domain ($r>0$) the deviations tend to 0, while for the decreasing case ($r<0$), the deviation grows with time. For sinusoidal growth, the deviations maintain oscillatory behavior with an amplitude proportional to $r\omega$; furthermore, the amplitude of

the deviations is affected by the distance between the frequency of the domain oscillation (measured by ω) and the frequency of the resulting chemical oscillation (measured by the imaginary part of the eigenvalues of $\mathbb{J}$).

All these features will be corroborated by our numerical simulations in the next section. However, the most important thing to note is that many of the scenarios result in situations where the homogeneous state tends to a constant value (exponential growth/shrinking), tends to the fixed point concentration (linear or quadratic growth), or maintains low amplitude oscillations around this concentration (oscillatory case), and in principle could be approximated by a constant value. This further approximation is considered in the next section.

3.4. Representative time-independent homogeneous state

The study of the homogeneous state is related to the search for Turing conditions for growing domains. These conditions can be expected to become significantly more complicated when the base state changes appreciably in time [30]. Furthermore, if we consider that the approximation to find these conditions is usually linear in spatial perturbations, it is expected that our estimation of the bifurcation will not respond immediately to abrupt temporal changes in the base state. Considering these two problems, in this work we also study the circumstances in which the base state can be approximated by a constant value.

Hence, we study the case where after a transient time given by the decay of the terms in $e^{\mathbb{J}t}$ in the deviations of Table 1, the solutions remain approximately the same during a time interval. In this case, an appropriate, constant value of the concentrations, let us call it $\mathbf{C}_0$, can capture the main qualitative features of the dynamics. This would simplify the (2.7) problem, since now the linear reaction term $\frac{\partial \mathbf{f}}{\partial \mathbf{c}}(\mathbf{C}_0)$ is time-independent. As we will demonstrate with numerical simulations, this approximation is valid when the growth rate r is sufficiently slow since in this case the inertial terms would be negligible.

Suppose that we are studying the Turing formation process on an interval $T = t_f - t_i$. If $\mathbf{c}_s(t)$ does not change much in T, a characteristic value of the concentrations can be their time average:

$$\mathbf{C}_0 = \frac{1}{t_f - t_i}\left(\int_{t_i}^{t_f} \mathbf{c}_s(t)\, dt\right). \tag{3.7}$$

The formal calculation of these integrals for most of the dynamics studied here is possible using (3.6) and Table 1. However, it involves large expressions in terms of special functions whose complexity adds nothing to the physical idea and therefore we do not explicitly write their value.

A notable exception is exponential growth where (3.7) leads to

$$\begin{aligned}\mathbf{C}_0 =& \Big[\mathbb{I} + r(\mathbb{J} - r\mathbb{I})^{-1} \\ &+ r(\mathbb{J} - r\mathbb{I})^{-2}\left(\frac{e^{\mathbb{J}t_i}e^{-rt_i} - e^{\mathbb{J}t_f}e^{-rt_f}}{t_f - t_i}\right)\Big]\mathbf{c}_0.\end{aligned} \tag{3.8}$$

Thus, if the eigenvalues of $\mathbb{J}$ have a negative real part, then $\mathbf{C}_0 \approx \left[\mathbb{I} + r(\mathbb{J} - r\mathbb{I})^{-1}\right]\mathbf{c}_0$ after the transient time.

For linear and quadratic growth with $r > 0$, if the eigenvalues of $\mathbb{J}$ have a negative real part, after a transient time, the deviations tend to zero, and therefore for $t \gg 0$ it follows that

$$\mathbf{C}_0 \approx \mathbf{c}_0, \tag{3.9}$$

and it is safe to take the fixed-point concentrations for sufficiently long times.

For sinusoidal growth, if the eigenvalues of $\mathbb{J}$ have negative real parts far from zero, the periodic functions of $\boldsymbol{\delta C}(t)$ average zero over all intervals that are multiples of $2\pi/\omega$. Thus, for low values of $|r|$ and a time interval consisting of integer periods, the concentration deviation oscillates with small amplitudes, and therefore the approximation (3.9) can also be used.

In this section we have studied the assumption that concentration changes are negligible over an interval. This will depend on the type and rate of growth, the chemical reaction, and the proximity to the bifurcations. In the next section we will propose some criteria and exemplify their use for the Brusselator, showing through numerical simulations the scope of these approximations.

4. A study case: The Brusselator

To check the accuracy of the approximations, we study here the base state of the Brusselator system, Eqs. (2.3). This is an example of a reaction system where the fixed point is not the origin. To simplify our study, the parameters used and the bifurcation analysis coincide with those of Ref. [26], and are summarized in the following lines. The Brusselator has a single fixed point at $\mathbf{c}_0 = (A, B/A)$ and realizes a stability change via a Hopf bifurcation at $B = B_H = 1 + A^2$, when the system describes a limit cycle. The Turing conditions for a fixed-size domain require a low value for the diffusion coefficient ratio, $\sigma = D_u/D_v$. For example, if $A = 1$ and $\sigma = 0.1$, the Turing bifurcation occurs at $B_T = 1.732$ and the Turing region is between $B_T \leq B < B_H$ and $B_H = 2.0$. For our study, we will use these values while varying B and r to highlight the influence of bifurcation distance and growth rate. We expect the Turing conditions in the growing domain to evolve gradually as a function of r.

4.1. General features of the base state

In Figure 1, we present the numerical solutions of Eqs. (2.6) when $B = 1.75$. Both concentrations (c_u, c_v) are represented by solid lines with colors distinguishing three different values of r, red for shrinkage and green and blue for growth. The dashed curves show the base state as predicted by our approximation in equation (3.3). The subfigures correspond to the linear, quadratic, exponential, and periodic dynamics of the domain, respectively. For comparison, we also plot in gray horizontal dotted lines the fixed point concentrations $\mathbf{c}_0$, which would be the value to which the concentrations would tend in a domain of fixed size. This value is used as the initial condition. The results in Figure 1 show the following:

- For both linear and quadratic growth (the first and second columns of Figure 1), the solutions exhibit an initial burst, and then asymptotically tend toward the fixed point concentrations $\mathbf{c}_0$, slower for quadratic than for linear. The amplitude of this outburst appears proportional to the value of r. For both linear and quadratic shrinkage, the initial solutions remain close to $\mathbf{c}_0$ at first, and as the domain sizes approach zero, the concentrations begin to move away from the fixed-point value, growing indefinitely as the domain tends to zero size.

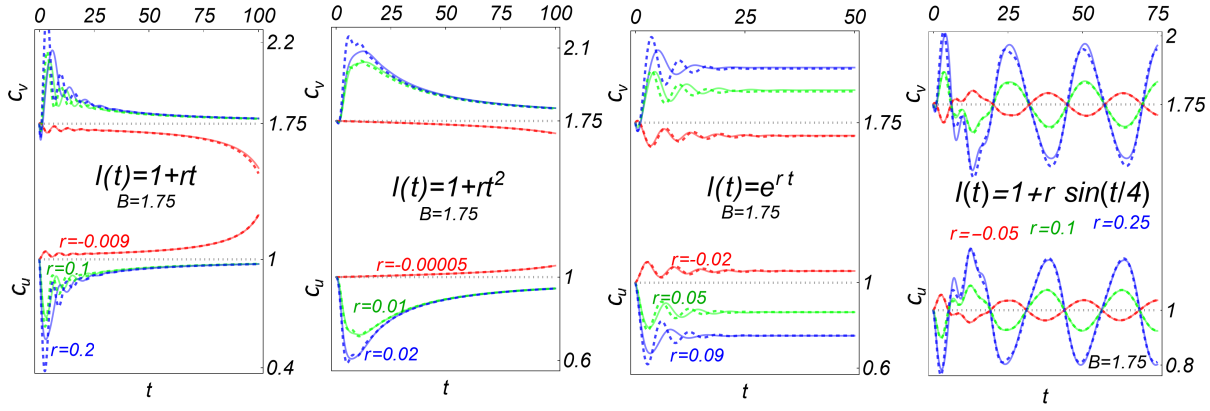

Figure 1. Base state of the Brusselator with $B = 1.75$. Each column represents different growth rates given in the inset. Solid lines: direct numerical solution of (2.6). Dashed lines: linear approximation in (3.3). Different values of parameter r are represented by colors, blue and green for growth and red for shrinking. Fixed-point concentrations are gray dotted lines.

- In the exponential growth/shrinkage case (third column of Figure 1), after a short initial burst, the solutions asymptotically tend to a constant value different from $\mathbf{c}_0$. The distance between the asymptotic and fixed-point concentrations grows with the absolute value of r. This tendency to an asymptotic value appears to occur more rapidly than with the other types of growth studied.
- In the case of sinusoidal growth (the fourth column of Figure 1), the size change produces concentration oscillations with the same frequency as the domain changes, ω. The amplitude appears proportional to the absolute value of r. After an initial transient state, where several frequencies can be identified, the oscillations occur periodically with a single period $2\pi/\omega$. These statements summarize the main variations of the homogeneous state concerning the parameter r.

Figure 2 replicates the results of Figure 1 ($B = 1.75$) for $B = 1.1$ and $B = 1.9$, examining the effect of proximity to the Hopf bifurcation at $B_H = 2$ for $r = 0$. The comparison reveals that for both linear and quadratic growth, the amplitude of the initial outburst increases with B, meaning that as the system approaches the Hopf bifurcation, transient oscillations become more numerous and prolonged. Stable concentrations are reached more quickly for values of B closer to B_H. In the exponential case, lower values of B lead to a faster approach to the steady state, while the initial deviation from the fixed-point concentration grows with B. Under sinusoidal growth, oscillation amplitudes around the fixed-point concentration increase with B.

4.2. Validity of the time-dependent approximation in (3.3)

As equation (3.3) is a linear approximation to the nonlinear problem in (2.6), it is expected to be appropriate when the system is far from unstable states and has a small growth rate. The first of these conditions requires B smaller than the value of the Hopf bifurcation, and the second requires a small dilution term (proportional to r in absolute value). This is corroborated in all the comparisons between the direct numerical solution for the base state (solid lines) and its approximation (dashed lines) in Figs. 1–2. The scope of these two limitations of the model can be quantified as follows.

For each type of growth, we compare the numerical solution in (2.6) with the solution in (3.3) by

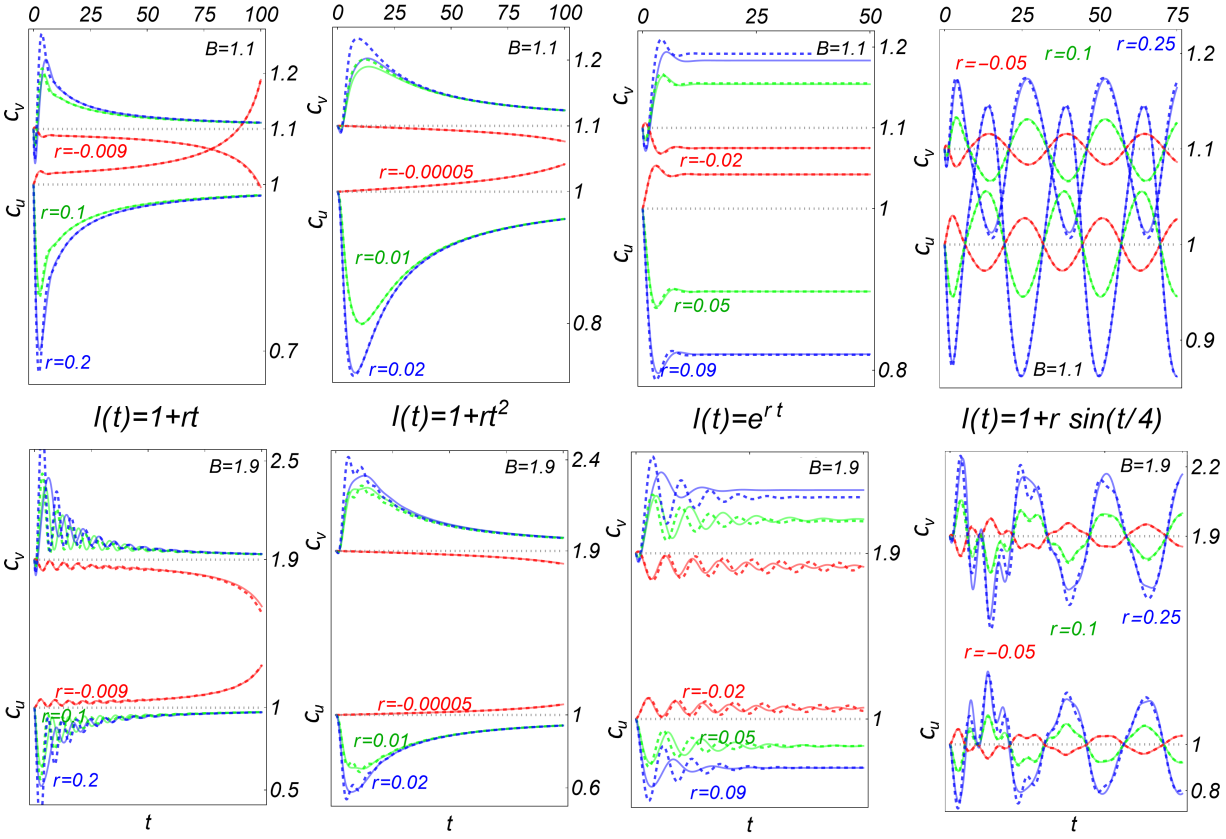

Figure 2. Homogeneous state of the Brusselator with $B = 1.1$ (top) and $B = 1.9$ (bottom). The same instructions apply as in Figure 1.

varying the growth parameter r. For linear, quadratic, and exponential growth, we increase the value of r from zero until both solutions differ by up to 10%. This percentage error is the time-averaged difference of both solutions between time 0 and a maximum t_{max}. For growth, we define this as the time required for the domain to grow to ten times its original length, $l(t_{max})/l(0) = 10$. In contrast, for a contraction, $l(0)/l(t_{max}) = 10$, and t_{max} is the time required to shrink to ten times the original size. This difference is compared to the fixed-point value to provide a point of comparison for the magnitude of the error. The validity criterion for (3.3) is then

$$error_1 = \frac{1}{t_{max}} \int_0^{t_{max}} \frac{|\mathbf{c}(t') - \mathbf{c}_s(t')|}{|\mathbf{c}_0|} dt' < 10\%. \tag{4.1}$$

Figure 3 shows the validity regions of equation (3.3) for the Brusselator model under different growth types. The symbols indicate the maximum and minimum values of r for which equation (3.3) remains valid. As expected, its validity is restricted to low $|r|$ values and diminishes as the system moves away from the Hopf bifurcation. Additionally, the asymmetric profile reveals a broader applicability for growth compared to shrinkage.

For sinusoidal growth, there are two parameters, r and ω. Therefore, we modify both parameters starting at 0 until the numerical solution of (2.6) and (3.3) varies by 10%. The criterion is the same as in (4.1), but now t_{max} is the time needed for the system to oscillate six times, or $t_{max} = 6 \cdot (2\pi/\omega)$.

The results of this validation are visualized as the region in Figure 3(b), where it is shown that the approximation has higher validity for values of B far from the Hopf bifurcation. Moreover, there is some inverse relationship between the values of r and ω, which means that for values of $|r| \lesssim 1$ (large amplitude oscillations), the periodicity of domain size changes has to be slow; and for $|r| \approx 0$ (low amplitude oscillations), the domain oscillating frequencies can be higher.

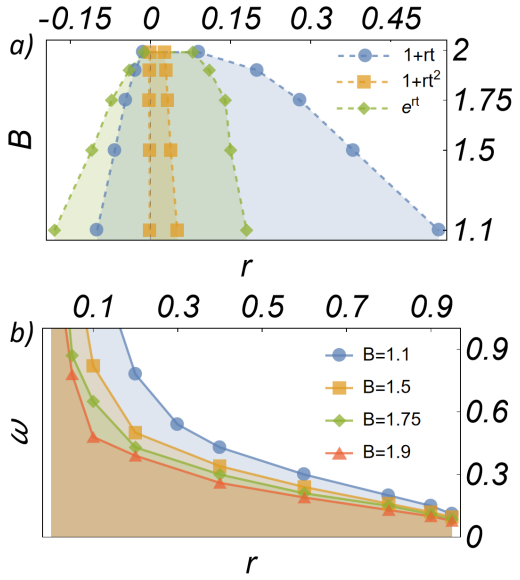

Figure 3. Regions of validity of the approximation (3.3) to the solution of (2.6) according to the criterion in (4.1). the top shows the types of growth in the inset and the bottom shows a periodic change in the size of the domain.

To physically understand the range of applicability of the scheme, let us exemplify what happens with exponential growth. Here the value of r is directly $\dot{l}(t)/l(t)$, the dilution rate; in terms of finite differences this means $\frac{\delta l(t)}{l(t)\delta t} = r$, and therefore $r \times 100$ represents the percentage of increase/decrease of the domain per unit of time. From Figure 3(a), it is observed that for exponential growth with $B = 1.75$, the scheme is valid until reaching $r \sim 0.1$; this means that (3.3) approximates a system that increases up to ten times its size in each unit of time. To determine whether growth is fast or slow, one would compare the value of r^{-1} (which gives a characteristic time for growth) with the characteristic times for diffusion and reaction. In general, this is the case for Turing patterns in biological systems, and therefore our approach is applicable. A similar reasoning can be applied to the other types of growth, as done in [18].

4.3. Validity of the time-independent approximation in equation (3.7)

In this section we will develop a criterion to know when the approximation of constant base state in (3.7) is valid. In Figure 4, we test the validity of equation (3.7) to approximate the direct numerical solution of the base state in equation (2.6) by measuring their difference according to the following error criterion:

$$error_2 = \frac{1}{2\,t_{max}/3} \int_{t_{max}/3}^{t_{max}} \frac{|\mathbf{c}(t') - \mathbf{C}_0|}{|\mathbf{c}_0|} dt' < 5\%. \tag{4.2}$$

In this way, we compare only the last two-thirds of the process and neglect the transient states up to $t_i = t_{max}/3$. As before, the choice of the maximum time t_{max} depends on the type of dynamics of the domain and whether it is growing or decreasing. The validity criterion we have chosen of 5% is stricter than the previous one because it considers a smaller time range.

The results of these comparisons are in Figure 4. It is concluded that for the linear, quadratic, and exponential cases, the (3.7) approximation applies for low values of $|r|$ and over a wider range of B values. In contrast to the comparison made with the time-dependent solution (3.3) in Figure 3, the constant approximation (3.7) is valid over a smaller range, with a more drastic reduction for a shrinking domain.

For the case of oscillatory variation of the domain, we note that the base state consists of oscillations around $\mathbf{c}_0$ with amplitude proportional to r and therefore, if n is the number of oscillations in time t_{max}, it is sufficient to have nr/ω small enough to satisfy this criterion. Therefore, for this type of growth, we do not run simulations to test the criterion in (4.2) since it depends on n.

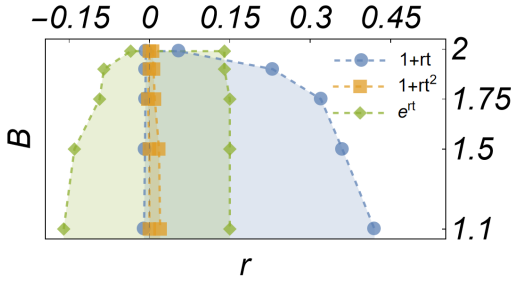

Figure 4. Regions of validity of the (3.7) approximation to the (2.6) solution according to the criterion in (4.2) for the growth functions in the inset.

In order to better visualize the tolerance criteria defined in (4.1) and (4.2), some comparisons of the numerical solutions of (2.6), the approximation $\mathbf{c}_s$ in (3.3) and $\mathbf{C}_0$ in (3.7), as well as the fixed-point concentrations $\mathbf{c}_0$ are shown in Figure 5. The parameters used for the simulations correspond to those in which the maximum error is committed according to both criteria. As can be observed, the similarity between the solutions in the interval defined by each criterion seems mostly acceptable.

The criteria introduced in (4.1) and (4.2) for estimating the numerical error are of a general nature and should be regarded as illustrative rather than exhaustive. Figures 3 and 4 delineate the applicability range of our numerical approximations in terms of the bifurcation parameter B and the growth/decay rate r for the Brusselator model. It is reasonable to expect that similar behaviors may arise in other reaction systems, since the error formula presented in Sec. 3.2 predicts validity whenever $|r|$ remains moderate compared to the damping rate of chemical perturbations—and depends on the growth regime, while requiring parameters to be sufficiently distant from the Hopf bifurcation (where the real part of the eigenvalues vanishes). Although it is generally difficult to anticipate the precise validity domain for an arbitrary reaction system, a preliminary numerical analysis can always be performed to assess it. One might therefore question the advantage of using the approximation scheme if such a preliminary

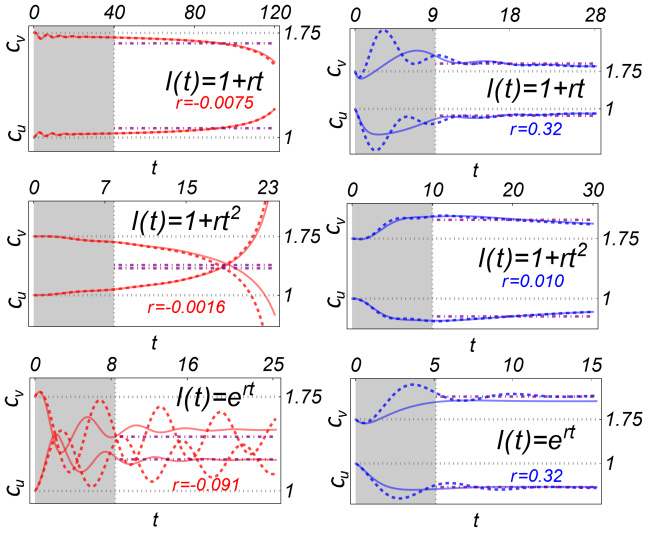

Figure 5. Comparison of $\mathbf{c}_s$ in (2.6) (solid lines), its approximation in (3.3) (dashed lines), $\mathbf{C}_0$ in (3.7) (magenta lines), and fixed-point concentrations $\mathbf{c}_0$ (gray dots). The region in gray is the one excluded for the calculation of the representative solution in (3.7).

study is already necessary to determine the steady-state solution. The strength of our approach lies precisely at this point: once the preliminary analysis is carried out, the analytic expression for $\mathbf{c}_s$ can be systematically employed in the formal conditions for the onset of Turing instabilities in expanding domains, thus providing a powerful predictive tool beyond specific numerical simulations.

The selection criteria in each case will depend on the time interval of interest, as well as the sensitivity of the system to changes in chemical concentrations. However, in this section we have shown that our two approximations in Eqs. (3.3) and (3.7) can be used to determine the base state over a relatively wide range of parameters. However, caution is needed when analyzing Turing pattern formation, as early-stage variations may influence the stability of initial spatial perturbations in ways not captured by the time-independent base state approximation. Hence, before making a study on the formation of Turing patterns on growing domains, it is advisable to make a prior analysis of the base state.

5. An approximation to the stability of the perturbations

The base state of the RDD equation plays a fundamental role in the stability of perturbations, as the system must remain stable in the absence of diffusion for Turing patterns to emerge. This section examines the impact of dilution on the stability of chemical reactions, drawing a comparison with a fixed-volume reactor. We begin by highlighting the inherent challenges of this problem.

The primary objective of this study is to approximate the base state described by equation (3.2) and summarized in Table 1 for different growth types. These analytical approaches will allow the explicit evaluation of Turing conditions in growth domains, conditions that have so far only been evaluated numerically [30]. That work also establishes stability conditions for the base state in the absence of diffusion using a Lyapunov-type potential function. These conditions are intricate and best analyzed within the broader framework of Turing instability discussed there. Our approach here aims for a more intuitive understanding of base state stability. Specifically, we seek to explain when the stability of a

reactive system in a fixed domain can be extended to a growing domain.

The key difficulty to solve this problem arises from the form of equation (6) for the base state. Any linearization of the reaction directly from (2.6) involves a Jacobian matrix evaluated in a time-dependent state. This poses a challenge because, in a linear system where the proportionality matrix varies with time, eigenvalues alone do not determine stability [42]. To show this, counter examples are found such that certain matrices have constant eigenvalues with negative real parts, yet their corresponding differential equations yield solutions that grow over time [43, 44]. As a result, proving the stability of the base state solely from the eigenvalues obtained via direct linearization of (2.6) is inconclusive. Such counterexamples are not common and they appear to belong to a specific class of non-autonomous systems with particular geometric properties, as studied in [45, 46].

Therefore the strategy followed in this work is approximate. Instead of studying the non-autonomous linear system suggested in equation (2.6) we use the approximation made in Section 2 where, as we showed from numerical simulations, the base state is very close to a constant concentration. This is of course only valid in the cases studied there, but they are general enough to outline some hypotheses about the possible effects of dilution.

So, let us consider the effect of homogeneous perturbations, $\boldsymbol{\zeta}_0(t)$. From equation (2.7), they obey

$$\frac{\partial \boldsymbol{\zeta}_0}{\partial t} + \frac{\dot{l}(t)}{l(t)}\boldsymbol{\zeta}_0 = \frac{\partial \mathbf{f}}{\partial \mathbf{c}}(\mathbf{c}_s)\boldsymbol{\zeta}_0. \tag{5.1}$$

This equation is explicitly time-dependent via $\mathbf{c}_s(t)$. To simplify the analysis, we consider the approximation where $\mathbf{c}_s(t) \approx \mathbf{C_0}$ in a time interval T, as validated by the growth rates and parameters in Figure 4. Further approximation can be done by assuming then than the time-dependent matrix $\frac{\partial \mathbf{f}}{\partial \mathbf{c}}(\mathbf{c}_s)$ can be approximated by $\hat{\mathbb{J}} \equiv \frac{\partial \mathbf{f}}{\partial \mathbf{c}}(\mathbf{C}_0)$, a constant matrix. If we multiply (5.1) by $l(t)$, this leads to the autonomous problem

$$\frac{\partial [l(t)\boldsymbol{\zeta}_0]}{\partial t} = \hat{\mathbb{J}}[l(t)\boldsymbol{\zeta}_0], \tag{5.2}$$

for the vector $\hat{\boldsymbol{\zeta}}_0 \equiv l(t)\boldsymbol{\zeta}_0$.

Let $\hat{\mathbb{P}}^{-1}$ be the modal matrix of $\hat{\mathbb{J}}$ and let $\hat{\mathbf{\Lambda}}$ be its diagonal eigenvalue matrix; they satisfy the property $\hat{\mathbf{\Lambda}} = \hat{\mathbb{P}}^{-1}\hat{\mathbb{J}}\hat{\mathbb{P}}$. Following the same lines of Section 3.1 and Appendix A in the Supplementary material, it can be shown that the perturbations in the absence of diffusion obey:

$$\boldsymbol{\zeta}_0(t) = \frac{l(0)}{l(t)}\hat{\mathbb{P}}^{-1}e^{\hat{\mathbf{\Lambda}}t}\hat{\mathbb{P}}\boldsymbol{\zeta}_0(0). \tag{5.3}$$

In this equation, the eigenvalues in the exponential matrix are those of the constant Jacobian matrix evaluated at $\mathbf{C}_0$ and not in $\mathbf{c_0}$, as in a fixed domain.

According to Turing's conditions, perturbations must be stable in the absence of diffusion. On a fixed-size domain, this condition requires $\mathcal{R}e[\Lambda_i] < 0$, that is, the real part of all eigenvalues of the diagonal matrix associated with the Jacobian at the fixed point $\mathbf{c}_0$ need to be negative. However, on a growing domain, this condition applied to (5.3) leads to:

$$\lambda_i(t) \equiv \mathcal{R}e[\hat{\Lambda}_i] - \frac{1}{t}\log\frac{l(t)}{l(0)} < 0 \tag{5.4}$$

for all components numbered by i and $t \in T$. Equation (5.4) follows directly from writing all the components of eq. (5.3) separately, writing the growth $l(t)$ as $\exp(\log(l(t)))$, and remembering that $\hat{\Lambda}$ is a diagonal matrix. This equation expresses approximately the growth rate behavior of perturbations when the base state does not change significantly in a time interval. It should be emphasized that $\lambda_i(t)$ does not constitute the computation of the time-dependent eigenvalues of the non-autonomous problem in (2.6), but only the solution of the approximate autonomous problem in (5.1).

This result in (5.4) establishes that spatial homogeneous perturbations will be damped if the local production of the chemical components (quantified by $e^{\hat{\Lambda}_i t}$) grows more slowly than the domain (quantified by $l(t)$), which is reasonable and reflects the effect of dilution. The local production rate is also affected by dilution, resulting in the modification of the base state $\mathbf{c}_0 \to \mathbf{C}_0$, and hence, of the eigenvalues $\Lambda_i \to \hat{\Lambda}_i$.

The approximate criterion for stability of perturbations in (5.4) presents some interesting and interpretable features and predictions:

- For a growing domain ($l(t)/l(0) > 1$), dilution causes states with stable parameters in a fixed domain to become more stable, i.e., to decay faster to their steady state: In physical terms, the consumption in a reaction is brought under control more rapidly toward a steady state due to the increase in volume. Furthermore, in contrast to a fixed domain, where a positive eigenvalue necessarily reflects instability, for an increasing domain, dilution can make it stable. Thus, chemical production can be outpaced by dilution, and although the number of molecules produced continues to increase, the concentration decreases if the volume grows more rapidly.
- For a shrinking domain where $l(t)/l(0) < 1$, the consequences are opposite, and in general, dilution makes states less stable. This may mean, first, that chemical damping may become slower due to domain contraction, and second, even that a stable perturbation in a fixed domain where $\mathcal{R}e[\Lambda_i] < 0$ may grow with time if the domain is shrinking very fast, as decreasing volume leads to increasing concentration.
- However, it is worth noting that dilution also modifies the steady-state concentrations. As we have observed in our simulations, this change is more pronounced for large values of the parameter measuring the growth rate (r in our case) and for chemical parameters close to the Hopf bifurcation (B_H in our case). In physical terms, this means that the growth/shrinkage effect is also capable of changing the local properties of the reaction, making it possible to change the stability of homogeneous perturbations.

To illustrate this, in Figure 6 we plot the value of $\lambda(t) \equiv \max\{\lambda_i\}$, where λ_i are defined in (5.4) for the case of linear growth $l(t) = 1 + rt$ for different values of r represented by different colors, red (shrinking), and green and blue (growing). The chosen values of r and B lie within the region where the approximation of $\mathbf{C}_0$ in equation (3.7) is valid according to the criterion in equation (4.2).

For $B = 1.75$ in Figure 6(a), we plot the most common situation in our simulations, where the rate $\lambda(t)$ remains negative if the original eigenvalues Λ_i have a negative real part, even in shrinking domains ($r < 0$). In these cases, the stability of the state $\mathbf{c}_0$ is inherited by $\mathbf{C}_0$, as can be seen in the second and third columns where we plot concentrations and perturbations, respectively. This seems to be the most common situation where the stability of the chemical reaction in the fixed domain is preserved for the growing domain.

However, in Figure 6(b) with $B = 1.99$ we show a situation where there may be a change in stability

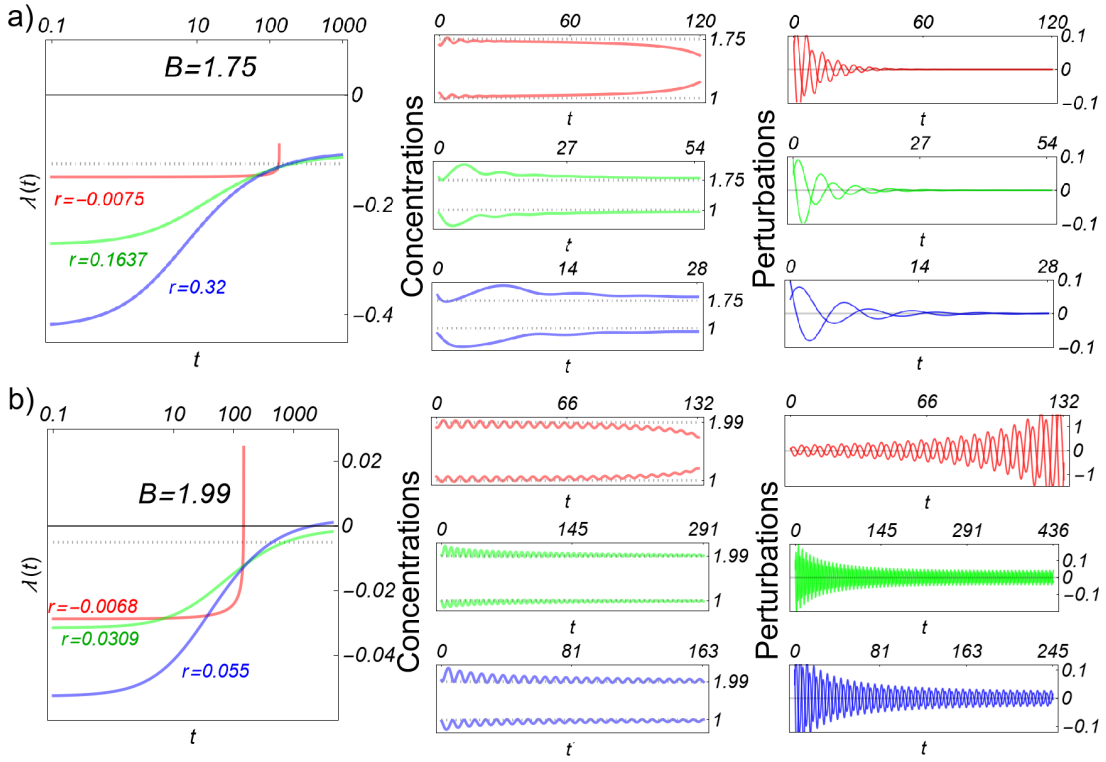

Figure 6. Brusselator perturbations with linear growth $l(t) = 1 + rt$ for a) $B = 1.75$ and b) $B = 1.99$. Left: Rate $\lambda(t)$ in (5.4) for each value of r (red, blue, and green solid lines) and the maximum eigenvalue of the reactive system in a fixed domain (grey dots). Center and Right: Numerical solutions for the homogeneous state in (2.6) and perturbations in (5.3), respectively.

due to the combined effect of high values of $|r|$ and proximity to a Hopf bifurcation. For this choice of parameters, the rate $\lambda(t)$ may start to grow until it becomes positive causing the perturbation $\boldsymbol{\zeta}_0$ to become unstable, both in growing (blue) and shrinking (red) domains. To show that this change in stability occurs due to dilution and not as a result of the approximations made in (5.4), in Figure 6(b), we also plot the perturbation (5.1) using $\mathbf{c}_s(t)$ obtained directly from numerical simulations of (2.6), showing that the concentration growth predicted by $\lambda(t)$ in this section is in general adequate.

Generality of the conclusions and comparison with the BVAM system

As mentioned above, different types of systems arise from different assumptions about the reactor. The Brusselator in equation (2.3) assumes a continuous feed with a constant rate A at concentration c_u leading to a non-equilibrium steady state given by $(A, B/A)$. In the case of the BVAM in equation (2.4), under appropriate parameters, it assumes the origin as the only equilibrium point and can therefore be interpreted as an equilibrium system or more generally as a reaction already centered in some constant state. This difference leads to significant differences in the behavior of the base state and the associated perturbations.

The first difference, according to the approximation in equation (3.3), is that the origin $\mathbf{c}_0 = \mathbf{0}$ still defines the asymptotic base state even for growing systems. This implies that for large times, the constant approximation in (3.7), $\mathbf{C}_0 \approx \mathbf{0}$, can be used. A second difference is that for the BVAM system, if the homogeneous state is asymptotically stable, according to (5.4), the only way the stability of perturbations can change is through shrinkage cases. The last difference concerns the ability of both systems to respond to perturbations: In our numerical experiments, we noticed that concentration changes from $\mathbf{c}_0$ in the Brusselator seem to increase the stability range of perturbations, that is, a system that is stable when $r = 0$ changes its state upon growth to maintain stability. This feature seems to be missing in the BVAM where it seems easier to find unstable perturbations in systems that would be stable in a fixed domain. For more details on these differences, see Appendix C of the Supplementary material.

6. Discussion and conclusions

We have studied in detail the base state resulting from reaction and diffusion processes in a one-dimensional growing domain. We present a scheme that allows us to predict that the effects of the dilution on the dynamics are as follows: 1) the base state is now time-dependent; 2) the steady-state concentrations may be different from the fixed-point concentrations expected for a fixed domain; and 3) the stability properties of perturbations may change due to local volume changes. Although this deduction is made for isotropic growth in one dimension, it is expected that in more dimensions it will present these same features.

To predict the spatial-homogeneous state we proposed a solution based on a linear approximation which we demonstrated correctly incorporates the above-mentioned features. This approximation is valid when the domain growth is slow, and for systems where the reaction parameters are below the Hopf bifurcation. The applicability of our approximation was verified with an extensive comparison against numerical solutions for the base state of different growth types: linear, quadratic, exponential, and oscillatory, although it is valid for any type of growth as long as it is slow.

We have shown that the steady state deviates from the chemical fixed-point concentrations due to

dilution, mainly in non-equilibrium systems where the fixed-point concentration of the reaction is not zero. This change in the steady-state concentration occurs especially for exponential growth. We show that after some time, a system with linear or quadratic growth tends to recover the concentrations it would have in the absence of growth, while oscillatory dynamics produce periodic oscillations of the same frequency around the fixed-point concentrations.

It is worth mentioning that the importance and applicability of our predictions for the homogeneous state lies in the search for Turing patterns. In this sense, we show that the stability of perturbations in a fixed domain is inherited in most cases from the stability of the steady state. However, we also show some counterexamples of the change in stability due to dilution, so it should be taken into account that the type of chemical system (position of the fixed point), as well as the shrinkage or proximity to the bifurcation, can modify the regions of the parameter space where Turing's first condition is applicable. To understand this effect, we have also deduced a linear approximation that allows quantifying the growth rate of perturbations that, for the parameters and the system studied, was effective in predicting the stability of perturbations, as corroborated with numerical simulations.

Regarding the Turing conditions for the appearance of spatial patterns, in this work, we discuss only the one related to stability in the absence of diffusion and establish that in a growing domain, stability depends on three factors: the change in concentrations at the steady state, the change in local volume that affects the concentration, and the stability that the chemical reaction would have in the absence of growth. The competition between these factors provides richer conditions for the appearance/disappearance of spatial patterns than those found in a fixed domain where only the fixed point is a determinant.

It is worth emphasizing that the primary significance of this study lies in the application of the homogeneous steady-state calculation to the analytical Turing conditions. In this sense, our results provide a complementary step that enables the formulation of preliminary criteria for the onset of Turing patterns, similar to those reported in [30], in which the evaluation of the predictions required numerical evaluation of the homogeneous state, $\mathbf{c}_s(t)$. In contrast, when an analytical approximation for $\mathbf{c}_s(t)$ is available, one can explicitly assess the accuracy of the predictions for the Turing conditions, as demonstrated in [47]. It should be noted that the full computation of the conditions governing the emergence of Turing patterns is beyond the scope of the present work. Nevertheless, such computations can be carried out either through estimates based on the time evolution of the Laplace–Beltrami spectrum [30] or by means of a Lyapunov function approach [47], both of which ultimately rely on the determination of $\mathbf{c}_s(t)$ obtained here. This underlines the importance of the present contribution.

One important thing to note is that the formal results given here for the homogeneous state and perturbation stability are general and can be applied to many-component chemical systems. While the results of this work are limited to systems whose linearization is diagonalizable, this constitutes the majority of physicochemical systems. Some of the theoretical tests were explicitly confirmed in the form of matrix components for two- and three-component systems. Furthermore, our predictions were also tested with numerical simulations of the homogeneous state for the Brusselator and BVMA reactions. Therefore, we believe that our results are robust and can be applied to predict the temporal base state of general RDD systems and help in future work to establish the conditions for the formation of Turing patterns in growing domains explicitly in terms of the parameters.

Author contributions

ALD conceived the study, developed the methodology, performed the calculations, and drafted the original manuscript. ISH and CGA validated the calculations, performed the simulations, and reviewed and edited the final manuscript.

Use of AI tools declaration

The authors declare they have not used Artificial Intelligence (AI) tools in the creation of this article.

Acknowledgments

A.L.D. acknowledges the financial support from the Universidad Nacional Autónoma de México (UNAM) through the projects FC-126526: Mathematical Modeling of Complex Physicochemical Systems and DGAPA-UNAM IA100126: Advanced Modeling and Machine Learning for Environmental Sustainability.

Conflict of interest

The authors declare there is no conflict of interest.

References

1. A. M. Turing, The chemical basis of morphogenesis, *Bull. Math. Biol.*, **52** (1990), 153–197. https://doi.org/10.1007/BF02459572
2. J. D. Murray, *Mathematical biology II: Spatial models and biomedical applications*, vol. 3, Springer, 2001. https://doi.org/10.1007/978-0-387-22437-4
3. E. Knobloch, R. Krechetnikov, Problems on time-varying domains: Formulation, dynamics, and challenges, *Acta Appl. Math.*, **137** (2015), 123–157. https://doi.org/10.1007/s10440-014-9989-9
4. L. Marcon, J. Sharpe, Turing patterns in development: What about the horse part?, *Curr. Opin. Genet. Dev.*, **22** (2012), 578–584. https://doi.org/10.1016/j.gde.2012.11.004
5. O. Chara, E. M. Tanaka, L. Brusch, Mathematical modeling of regenerative processes, *Curr. Top. Dev. Biol.*, **108** (2014), 283–317. https://doi.org/10.1016/B978-0-12-391498-9.00010-8
6. F. R. Macfarlane, M. A. J. Chaplain, T. Lorenzi, A hybrid discrete-continuum approach to model turing pattern formation, *arXiv*, ArXiv:2007.04195. https://doi.org/10.48550/arXiv.2007.04195 ,
7. C. Gilbert, T. Ellis, Biological engineered living materials: Growing functional materials with genetically programmable properties, *ACS Synth. Biol.*, **8** (2018), 1–15. https://doi.org/10.1021/acssynbio.8b00423
8. J. L. Payne, A. Wagner, The causes of evolvability and their evolution, *Nat. Rev. Genet.*, **20** (2019), 24–38. https://doi.org/10.1038/s41576-018-0069-5

9. I. Salazar-Ciudad, J. Jernvall, Graduality and innovation in the evolution of complex phenotypes: Insights from development, *J. Exp. Zool. B Mol. Dev. Evol.*, **304** (2005), 619–631. https://doi.org/10.1002/jez.b.21083
10. J. I. Overbø, Y. Ma, B. A. Edgar, Cell growth and the cell cycle: New insights about persistent questions, *BioEssays*, **44** (2022), e2200150. https://doi.org/10.1002/bies.202200150
11. M. B. Ginzberg, N. Chang, H. D'Souza, N. Patel, R. Kafri, M. W Kirschner, Cell size sensing in animal cells coordinates anabolic growth rates and cell cycle progression to maintain cell size uniformity, *eLife*, **7** (2018), e26957. https://doi.org/10.7554/eLife.26957
12. R. B. Haga, A. J. Ridley, Rho gtpases: Regulation and roles in cancer cell biology, *Small GTPases*, **7** (2016), 207–221. https://doi.org/10.1080/21541248.2016.1232583
13. C. D. Lawson, A. J. Ridley, Rho gtpase signaling complexes in cell migration and invasion, *J. Cell Biol.*, **217** (2018), 447–457. https://doi.org/10.1083/jcb.201612069
14. S. Hladyshau, J. P. Stoop, K. Kamada, S. Die, D. Tsygankov, Spatiotemporal coordination of rac1 and cdc42 at the whole cell level during cell ruffling, *Cells*, **12** (2023), 1638. https://doi.org/10.3390/cells12121638
15. M. Picard, R. J. Petrie, J. Antoine-Bertrand, É. Saint-Cyr-Proulx, J.-F. Villemure, N. Lamarche-Vane, Spatial and temporal activation of the small gtpases rhoa and rac1 by the netrin-1 receptor unc5a during neurite outgrowth, *Cell. Signal.*, **21** (2009), 1961–1973. https://doi.org/10.1016/j.cellsig.2009.08.017
16. M. Machacek, L. Hodgson, C. Welch, H. Elliott, O. Pertz, P. Nalbant, et al., Coordination of rho gtpase during cell protrusion, *Nature*, **461** (2009), 99–103. https://doi.org/10.1038/nature08242
17. W. A. Waters, R. A. Van Gorder, Turing patterns under hybrid apical–uniform domain growth, *Proc. R. Soc. A*, **481** (2024). https://doi.org/10.1098/rspa.2024.0935 .
18. A. Madzvamuse, E. A. Gaffney and P. K. Maini, Stability analysis of non-autonomous reaction-diffusion systems: The effects of growing domains, *J. Math. Biol.*, **61** (2010), 133–164. https://doi.org/10.1007/s00285-009-0293-4
19. T. Kolokolnikov, J. Wei, Pattern formation in a reaction-diffusion system with space-dependent feed rate, *SIAM Rev.*, **60** (2018), 626–645. https://doi.org/10.1137/17M1116027
20. A. L. Krause, E. A. Gaffney, B. J. Walker, Concentration-dependent domain evolution in reaction–diffusion systems, *Bull. Math. Biol.*, **85** (2023), 14. https://doi.org/10.1007/s11538-022-01115-2
21. C. Fraga Delfino Kunz, A. Gerisch, J. Glover, D. Headon, K. J. Painter, F. Matthäus, Novel aspects in pattern formation arise from coupling turing reaction–diffusion and chemotaxis, *Bull. Math. Biol.*, **86** (2024), 1–37. https://doi.org/10.1007/s11538-023-01225-5
22. L. Silva-Dias, I. R. Epstein, M. Dolnik, Turing patterns on rotating spiral growing domains, *Phys. Chem. Chem. Phys.*, **26** (2024), 26258–26265. https://doi.org/10.1039/D4CP02889A
23. S. Okuda, T. Miura, Y. Inoue, T. Adachi, M. Eiraku, Combining turing and 3d vertex models reproduces autonomous multicellular morphogenesis with undulation, tubulation, and branching, *Sci. Rep.*, **8** (2018), 1–15. https://doi.org/10.1038/s41598-018-20606-1

24. C. Konow, N. H. Somberg, J. Chavez, I. R. Epstein, M. Dolnik, Turing patterns on radially growing domains: Experiments and simulations, *Phys. Chem. Chem. Phys.*, **21** (2019), 6718–6724. https://doi.org/10.1039/C9CP00315A
25. R. Krechetnikov, E. Knobloch, Stability on time-dependent domains: Convective and dilution effects, *Phys. D*, **342** (2017), 16–23. https://doi.org/10.1016/j.physd.2016.10.005
26. A. Ledesma-Durán, E. Ortiz-Durán, J. Aragón, I. Santamaría-Holek, Eckhaus selection: The mechanism of pattern persistence in a reaction-diffusion system, *Phys. Rev. E*, **102** (2020), 032214. https://doi.org/10.1103/PhysRevE.102.032214
27. M. Ghadiri, R. Krechetnikov, Pattern formation on time-dependent domains, *J. Fluid Mech.*, **880** (2019), 136–179. https://doi.org/10.1017/jfm.2019.694
28. H. Kim, A. Yun, S. Yoon, C. Lee, J. Park, J. Kim, Pattern formation in reaction–diffusion systems on evolving surfaces, *Comput. Math. Appl.*, **80** (2020), 2019–2028. https://doi.org/10.1016/j.camwa.2020.08.029
29. S. T. Vittadello, T. Leyshon, D. Schnoerr, M. P. H. Stumpf, Turing pattern design principles and their robustness, *Philos. Trans. R. Soc. A*, **379** (2021), 20200272. https://doi.org/10.1098/rsta.2020.0272
30. R. A. Van Gorder, V. Klika, A. L. Krause, Turing conditions for pattern forming systems on evolving manifolds, *J. Math. Biol.*, **82** (2021), 1–61. https://doi.org/10.1007/s00285-021-01609-6
31. V. Klika, Significance of non-normality-induced patterns: Transient growth versus asymptotic stability, *Chaos*, **27** (2017), 073114. https://doi.org/10.1063/1.4996824
32. V. Klika, M. Kozák and E. A. Gaffney, Domain size driven instability: Self-organization in systems with advection, *SIAM J. Appl. Math.*, **78** (2018), 2298–2322. https://doi.org/10.1137/17M115843X
33. V. Klika and E. A. Gaffney, History dependence and the continuum approximation breakdown: The impact of domain growth on turing's instability, *Proc. R. Soc. A*, **473** (2017), 20160744. https://doi.org/10.1098/rspa.2016.0744
34. B. Pena and C. Perez-Garcia, Stability of turing patterns in the brusselator model, *Phys. Rev. E*, **64** (2001), 056213. https://doi.org/10.1103/PhysRevE.64.056213
35. R. A. Barrio, Turing systems: A general model for complex patterns in nature, in *Physics of emergence and organization*. World Scientific, 2008, 267–296. https://doi.org/10.1142/9789812814739_0011
36. A. Madzvamuse, Time-stepping schemes for moving grid finite elements applied to reaction–diffusion systems on fixed and growing domains, *J. Comput. Phys.*, **214** (2006), 239–263. https://doi.org/10.1016/j.jcp.2005.09.018
37. R. G. Plaza, F. Sánchez-Garduño, P. Padilla, R. A. Barrio, P. K. Maini, The effect of growth and curvature on pattern formation, *J. Dyn. Differ. Equ.*, **16** (2004), 1093–1121. https://doi.org/10.1007/s10884-004-7837-9
38. E. J. Crampin, E. A. Gaffney, P. K. Maini, Reaction and diffusion on growing domains: Scenarios for robust pattern formation, *Bull. Math. Biol.*, **61** (1999), 1093–1120. https://doi.org/10.1006/bulm.1999.0132

39. A. L. Krause, M. A. Ellis, R. A. Van Gorder, Influence of curvature, growth, and anisotropy on the evolution of turing patterns on growing manifolds, *Bull. Math. Biol.*, **81** (2019), 759–799. https://doi.org/10.1007/s11538-018-00557-w

40. M. Meixner, A. De Wit, S. Bose, E. Schöll, Generic spatiotemporal dynamics near codimension-two turing-hopf bifurcations, *Phys. Rev. E*, **55** (1997), 6690–6699. https://doi.org/10.1103/PhysRevE.55.6690

41. A. Ledesma-Durán, J. L. Aragón, Primary and secondary instabilities of the mixed mode solution in a reaction diffusion system near the codimension-two turing-hopf point, *Chaos Soliton. Fract.*, **124** (2019), 68–77. https://doi.org/10.1016/j.chaos.2019.04.038

42. H. K. Khalil, *Nonlinear Systems*, 3rd edition, Prentice Hall, 2002.

43. M. Wu, A note on stability of linear time-varying systems, *IEEE Trans. Automat. Contr.*, **19** (1974), 162. https://doi.org/10.1109/TAC.1974.1100520

44. E. Knobloch, W. Merryfield, Enhancement of diffusive transport in oscillatory flows, *Astrophys. J.*, **401** (1992), 196–205. https://doi.org/10.1086/172054

45. K. Josić, R. Rosenbaum, Unstable solutions of nonautonomous linear differential equations, *SIAM Rev.*, **50** (2008), 570–584. https://doi.org/10.1137/07069620X

46. J. Mierczyński, Instability in linear cooperative systems of ordinary differential equations, *SIAM Rev.*, **59** (2017), 649–670. https://doi.org/10.1137/16M1082778

47. A. Ledesma-Durán, C. García-Alcántara, I. Santamaría-Holek, Turing conditions for a two-component isotropic growing system from a potential function, *Results Appl. Math.*, **28** (2025), 100664. https://doi.org/10.1016/j.rinam.2024.100664

Supplementary material

Appendix A. Proof of equation (9)

Let us part from equation (3.1). Making the change $\delta\mathbf{c} = \mathbb{P}\mathbf{u}$, and multiplying equation (3.1) at the left for $\mathbb{P}^{-1}$, leads to the first order differential equation

$$\frac{d\mathbf{u}}{dt} + [g(t) - \mathbf{\Lambda}]\mathbf{u} = -g(t)\mathbb{P}^{-1}\mathbf{c}_0,$$

where all the components of $\mathbf{u}$ are uncoupled. This means that the method of integrating factor can be used. Multiplying this equation by the matrix $\exp[\int g(t') - \mathbf{\Lambda} dt']$ and using the fact that $\exp(\int g(t')dt') = l(t)$ given the definition of $g(t)$, the method leads to

$$\mathbf{u} = \frac{1}{l(t)}e^{\mathbf{\Lambda}t}\mathbf{U} - \frac{e^{\mathbf{\Lambda}t}}{l(t)}\left(\int_0^t l'(t')e^{-\mathbf{\Lambda}t'}dt'\right)\mathbb{P}^{-1}\mathbf{c}_0.$$

Here $\mathbf{U}$ is constant vector of integration. For determining its value, multiplying this equation by $\mathbb{P}$ and using again $\delta\mathbf{c} = \mathbb{P}\mathbf{u}$ results is an equation for $\delta\mathbf{c}$. Now using the initial condition for $\delta\mathbf{c}(0)$, it is possible to identify $\mathbf{U} = l(0)\mathbb{P}^1\delta\mathbf{c}(0)$, which leads to equation (3.2):

$$\delta\mathbf{c} = \frac{l(0)}{l(t)}\mathbb{P}e^{\mathbf{\Lambda}t}\mathbb{P}^{-1}\delta\mathbf{c}(0) - \mathbb{P}\frac{e^{\mathbf{\Lambda}t}}{l(t)}\left(\int_0^t l'(t')e^{-\mathbf{\Lambda}t'}dt'\right)\mathbb{P}^{-1}\mathbf{c}_0.$$

Appendix B. Base state for quadratic growth

Let $l(t) = l_0(1 + rt^2)$, where l_0 is the length of the fixed domain and r a parameter that measures how fast the domain grows. For this case, we can explicitly calculate for any i:

$$\frac{e^{\Lambda_i t}}{l(t)}\int_0^t e^{-\Lambda_i t'}l'(t')dt' = \frac{2r\left(-t\Lambda_i + e^{\Lambda_i t} - 1\right)}{\Lambda_i^2(1 + rt^2)},$$

as the Eqs. in (3.3) are decoupled and assuming that all eigenvalues are non zero. Since all involved matrices in (3.3) are diagonal, this means that

$$\frac{e^{\mathbf{\Lambda}t}}{l(t)}\int_0^t e^{-\mathbf{\Lambda}t'}l'(t')dt' = \frac{2r}{1 + rt^2}\left(-t\mathbf{\Lambda}^{-1} + \mathbf{\Lambda}^{-2}e^{\mathbf{\Lambda}t} - \mathbf{\Lambda}^{-2}\right).$$

Using systematically the property $\mathbb{J}^m = \mathbb{P}\mathbf{\Lambda}^m\mathbb{P}^{-1}$ (which implies $e^{\mathbb{J}} = \mathbb{P}e^{\mathbf{\Lambda}}\mathbb{P}^{-1}$), from (3.3) we obtain that:

$$\mathbf{c}_s = \left[\mathbb{I} - \frac{2r}{1 + rt^2}\left(-t\mathbb{J}^{-1} + \mathbb{J}^{-2}e^{\mathbb{J}t} - \mathbb{J}^{-2}\right)\right]\mathbf{c}_0.$$

Using the definition in (3.6), it is possible to obtain the deviation $\boldsymbol{\delta C}(t)$ in Table 1 for quadratic growth. For all other growth types the computations are performed in a similar fashion.

Appendix C. Differences between the The BVAM and Brusselator reactions

Eq. (3.3) allows us to predict that a system with the origin as the only fixed point ($\mathbf{c}_0 = \mathbf{0}$) cannot change the value of its steady homogeneous concentration. To exemplify this, we can use the BVAM in (2.4) which, with coefficients $a = -1$, $h = 3$, and $-3 < b < -1$, exhibits a single fixed point in the origin. The Hopf bifurcation occurs at $b_H = -1$, where the system has periodic oscillations [41].

In Figure 7, we plot the direct numerical solutions of the equation (2.6) using the BVAM in (2.4) (solid lines) and the analytical approximation in (3.2) (dashed) giving a good comparison and showing that our approximation is also valid. It should be noted that, in contrast to the Brusselator reaction, in the BVAM system all types of growth lead to the same asymptotic behavior.

Another aspect to highlight related to the position of the fixed point is associated with the stability of the base state and perturbations. In the BVAM system, if the base state is asymptotically stable, according to (5.4), the only way to destabilize the system corresponds to the shrinking. This is exemplified in Figure (8), where we repeat the analysis of Section 5 but now for the BVAM, plotting the results of (5.4) with the base state to the left and perturbations to the right. Since in this case $\mathbf{C}_0 = \mathbf{0}$, then $\lambda(t) = \mathcal{R}e[\mathbf{\Lambda}_i] - \log[l(t)/l(0)]/t$, and therefore, the dilution effect can increase the value of λ only if $l(t) < l(0)$. We exemplify this for linear growth in the BVAM system where the curves of λ are necessarily below the eigenvalue (grey line) for growing (green and blue cases) and above to shrinking

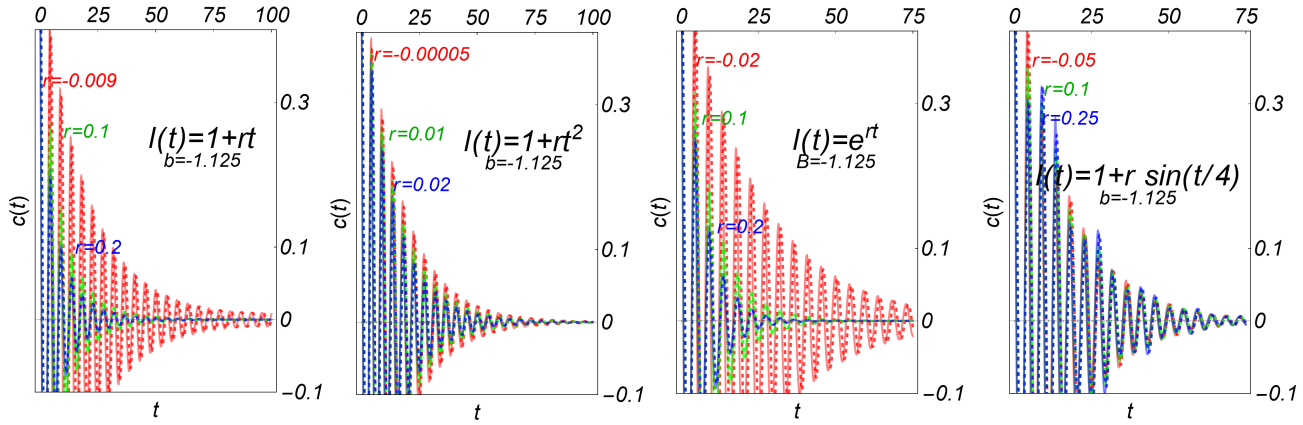

Figure 7. Homogeneous state for the first concentration of the BVAM with $b = -1.125$ using the direct solution of (2.6) (solid lines) and the approximation in (3.2) (dashed lines). The different types of growth are given in the inset of each column, and the values of r are distinguished by color: growth (green and blue) and shrinkage (red).

(red curve). This is in contrast to what occurs in Figure 6 for the Brusselator, where the curves of $\lambda(t)$ can be above and below the maximum eigenvalue.

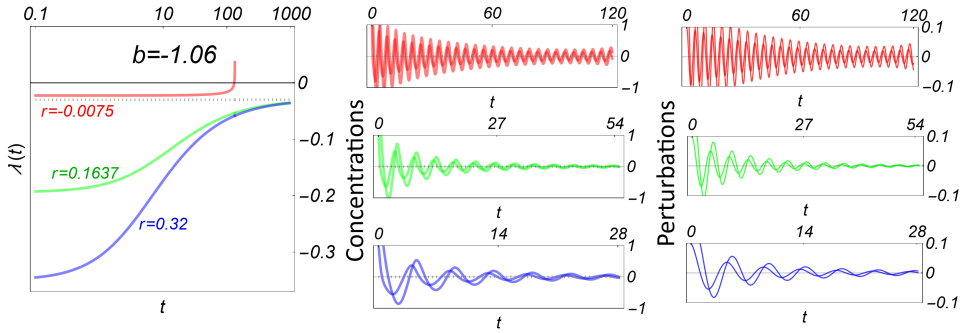

Figure 8. BVAM perturbations for $b = -1.06$ and linear growth $l(t) = 1 + rt$. The same instructions apply as in Figure 6.

One last aspect to comment on the differences between both systems refers to the stability of perturbations. In the case of the BVAM, there is no change in steady concentration, and the change in size causes the net rate $\lambda(t)$ to be above or below the maximum eigenvalue associated with the reaction. This is directly illustrated for exponential growth in Figure 9(a), where the decreasing domain (in red color) is capable of changing the stability of BVAM perturbations. In the case of the Brusselator, contrary to what might be expected for exponential growth, even for strong shrinkage, in our simulations we observe that the base state solution rarely loses stability if the solution is stable in a fixed domain. This is illustrated in Figure 9(b), where even for relatively large shrinkage (producing large differences between $\mathbf{c_0}$ and $\mathbf{C}_0$), the perturbations $\boldsymbol{\zeta}_0$ tend asymptotically to zero. In physical terms, this may suggest that the change in concentration of $\mathbf{c_0} \to \mathbf{C}_0$ caused by dilution is intended to preserve the stability of material production/consumption locally as the system grows or shrinks.

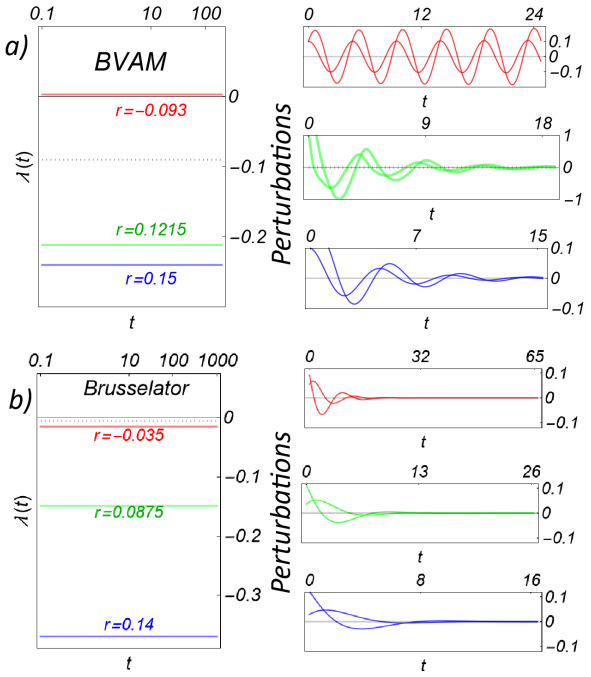

Figure 9. Behavior of the perturbations for a) the BVAM with $b = -1.18$ and b) the Brusselator with $B = 1.99$ for exponential growth with $l(t) = e^{rt}$. We show the predicted rate $\lambda(t)$ of each perturbation at the left sides of each figure for three different r values according to (5.4) (in red, green and blue colors) and the maximum eigenvalue of the fixed-domain problem. On the right sides, we plot the perturbations using the direct numerical solution of (5.1) with (2.6).